lubricants

MDPI

Article

Picosecond Laser Surface Texturing on Copper Substrates: Boosting Interfacial Adhesion and Tribological Performance of Magnesium Silicate Hydroxide-Based Solid Lubricant Coatings

Bo Gao [1], Hanzhi Yao [1], Qiuying Chang [1,*], Ruizhe Li [1], Zhongnan Wang [1], Xiangli Wen [2], Pengpeng Bai [3], Bin Wang [1] and Zhenyu Tian [4]

[1] School of Mechanical, Electronic and Control Engineering, Beijing Jiaotong University, Beijing 100044, China; gaobo1@bjtu.edu.cn (B.G.); 23222017@bjtu.edu.cn (H.Y.); 24221165@bjtu.edu.cn (R.L.); zhn.wang@bjtu.edu.cn (Z.W.); binwang1@bjtu.edu.cn (B.W.)
[2] Institute of Technology for Carbon Neutralization, Yangzhou University, Yangzhou 225127, China; xlwen@yzu.edu.cn
[3] State Key Laboratory of Tribology, School of Mechanical Engineering, Tsinghua University, Beijing 100084, China; baipengpeng@mail.tsinghua.edu.cn
[4] Shandong Metallurgical Machinery Factory Co., Ltd., No. 1 Xincun Road, Nanding Town, Zhangdian District, Zibo 255064, China; sdyjtzy@163.com
* Correspondence: qychang1@163.com

Abstract

Metal substrates were preprocessed via picosecond laser surface texturing (PLST, 532 nm) to fabricate interfacial microgrooves for tribological performance optimization prior to deposition of a magnesium silicate hydroxide (MSH)/graphite/MoS_2–PI solid lubricant coating. By tuning the PLST parameters (average laser power: 0.2–0.5 W, scan passes: 3–5, hatch spacing: 0.005–0.1 mm), three representative texture geometries (linear, circular, and square) were produced, and the resulting coating performance was compared with conventional mechanical polishing and sandblasting pretreatments. Among the three laser textures, the linear texture exhibited the most excellent tribological performance and interfacial adhesion, outperforming the circular and square counterparts. Ball-on-disk tests in a kerosene-contaminated environment (10 N, 800 rpm) showed that the linear-textured sample reached the lowest steady-state friction coefficient (0.038), lower than polished (0.048) and sandblasted (0.052) controls, together with reduced wear scar dimensions. Progressive-load scratch tests indicated a pronounced adhesion enhancement, with the critical failure load increasing from 7.05 N (polished) to 26.05 N for the linear-textured interface, which is higher than 21.21 N (circular) and 23.78 N (square) textures. Cross-sectional microscopy and EDS mapping reveal that the laser-defined microgrooves (~15 μm depth, ~120 μm width, ~500 μm spacing) act as a parameter-controlled interfacial architecture that promotes mechanical interlocking and provides lubricant-rich reservoirs. This laser-enabled interfacial design suppresses delamination, supports transfer film stability, and ultimately enhances the coating's tribological performance by reducing friction and wear.

Keywords: tribological performance; solid lubricant coating; substrate pretreatment; interface micro-grooves; friction and wear; picosecond laser surface texturing

Check for updates

Received: 13 March 2026
Revised: 2 April 2026
Accepted: 8 April 2026
Published: 10 April 2026

Copyright: © 2026 by the authors. Licensee MDPI, Basel, Switzerland. This article is an open access article distributed under the terms and conditions of the Creative Commons Attribution (CC BY) license.

1. Introduction

Friction and wear are critical factors leading to energy loss and mechanical failure, with approximately one-third of the world's energy consumed by friction and 70% of

large mechanical component failures caused by wear [1]. Solid lubrication technology has emerged as a reliable solution for extreme working conditions (high temperature, high pressure, vacuum, etc.) by forming boundary lubricating films to reduce direct contact between friction surfaces [2–5]. However, conventional solid lubricating coatings generally suffer from insufficient bonding strength with substrates and poor tribological performance under severe conditions such as heavy load and high speed.

Inspired by biological non-smooth surfaces, surface texturing technology has been proven effective in enhancing tribological properties by fabricating microstructures with specific patterns and dimensions on material surfaces [6–11]. When combined with solid lubricating coatings, surface textures can enable storage and release of lubricants, improve the bonding state between coatings and substrates, and synergistically enhance wear resistance [12,13]. Existing studies have explored a variety of preparation processes for solid lubricating coatings. Suitable process schemes need to be selected according to specific application scenarios, and these processes have a significant impact on the physicochemical properties of coatings. At present, the most widely used preparation methods mainly include mechanical coating, hot-press filling, organic resin bonding, and vapor deposition [14–18]. There are numerous surface texture machining methods (Electrical Discharge Machining (EDM), Electrochemical Machining (ECM), Ultrasonic Machining (USM), laser processing, etc.) [19–24], among which laser processing stands out due to its high precision and material adaptability. Studies have shown that laser-processed surface textures can effectively improve the bonding strength of substrates to coatings, forming an interlocking-like structure [25,26], but the effects of different texture types on the friction coefficient and wear life of coatings still need further investigation.

Ultrafast (picosecond/femtosecond) laser texturing enables flexible micro-patterning with a minimal heat-affected zone, making it well-suited for tailoring the surface topography of thermally sensitive metallic substrates [27–29]; laser-defined micro-textures can act as micro-reservoirs, debris traps, and lubricant-entrainment pathways while strengthening coating/substrate interfaces via mechanical interlocking [30–33]. Despite these merits, existing tribological studies on ps/fs laser texturing have focused primarily on conventional lubricant systems and clean (dry or oil-lubricated) environments. As a novel inorganic layered solid lubricant with excellent lamellar slip behavior and chemical stability, magnesium silicate hydroxide (MSH) exhibits promising friction-reducing performance in composite coatings [34,35]. This work aims to address the identified research gaps by revealing the synergistic effects of PLST and MSH-based coatings under kerosene-contaminated conditions, identifying the optimal texture geometry for copper substrates, and establishing a clear linkage among picosecond laser processing, interfacial architecture, and coating performance—ultimately providing a laser-enabled route to enhance solid lubricant coating reliability in severe sliding environments.

In this investigation, a picosecond laser surface texturing (PLST) pretreatment was applied to copper substrates to construct a controllable interfacial microgroove architecture prior to MSH-based solid lubricant coating deposition. The microstructures of the resulting coatings were systematically characterized, and their tribological response and interfacial adhesion were quantified. For benchmarking purposes, two conventional substrate pretreatment methods (mechanical polishing and sandblasting) were also implemented, and the resultant coatings were evaluated under identical test conditions [36]. By linking ultrafast laser processing, interfacial geometry, and coating performance, this work provides a laser-enabled surface-engineering route to improve the reliability of solid lubricant coatings under severe sliding environments.

2. Experimental Section

2.1. Coating Materials and Preparation

The solid lubricating coating prepared in this paper includes lubricating phases (nano-MSH, molybdenum disulfide, and graphite), reinforcement phases (nano-aluminum oxide and cerium fluoride), and a binder (polyimide resin). Among them, nano-MSH is an oxygen-containing salt formed by the combination of octahedral layers of magnesium cations and tetrahedral layers of silicate, with the chemical formula ideally expressed as $Mg_2[Si_4O_{10}](OH)_2$. Its chemical composition consists of 31.72% MgO, 63.52% SiO_2, and 4.76% H_2O. Specific information on other materials can be found in Table 1.

Table 1. Coating original material information.

Coating Composition	Name and Chemical Formula	Size	Manufacturer
Lubrication phases	Molybdenum disulfide (MoS_2)	<2 μm	Shanghai Aladdin Bio–Chem Technology Co., Ltd., Shanghai, China
	Graphite (C)	8000 mesh	Shanghai Macklin Biochemical Technology Co., Ltd., Shanghai, China
	MSH ($Mg_2[Si_4O_{10}](OH)_2$)	<2 μm	self-developed
Reinforcement phases	Alumina A (AL_2O_3)	20 nm	Shanghai Aladdin Bio–Chem Technology Co., Ltd., Shanghai, China
	Cerium fluoride (CeF_3)	3 μm	
Bonding phase	Polyimide ($(C_{22}H_{10}N_2O_4)n$)	-	Qinyang Tianyi Chemical Co., Ltd., Qinyang, China

The synthesis of the MSH-based composite coating entailed a multistep protocol:

1. High-energy mechanical homogenization of solid powders with a mass ratio of MoS_2: graphite: MSH: Alumina: Cerium fluoride = 5:2:5:0.4:1.2 to obtain the mixed lubricant materials.
2. Adding the mixed solid materials into the PI liquid dissolved in dimethylformamide solvent, meanwhile controlling the mass ratio of solid materials to PI equal to 1:2.
3. Setting atmospheric spraying parameters including pressure 0.48 MPa, and spraying distance 225 mm, implemented using the self-developed spraying machine shown in Figure 1a. The appearance of the prepared coating is shown in Figure 1b. The suspension mixture liquid was sprayed on the surface of copper after degreasing, surface activation (micro-roughening), polishing, and subsequent substrate pretreatment by picosecond laser texturing or sandblasting (details below).
4. Desiccation of the coating-coated copper substrate in air for 60 min to remove most of the solvent, followed by a drying phase within a vacuum furnace at 200 °C for 1 h.

A picosecond pulsed laser system (Figure 1c, picosecond pulsed laser) was used to fabricate textures of different shapes. The picosecond pulse regime was selected to achieve precise micro-texturing with minimal thermal damage on copper. The textures were written by galvanometer scanning under ambient conditions, and an in situ debris removal device was used to reduce particle redeposition. The experimental setup for ultrafast laser processing and the laser path primarily consist of a picosecond laser, a single-wavelength reflector, a beam expander, a quarter-wave plate, a lifting and steering frame, a scanning galvanometer, an F-theta field lens, and a debris removal device. For the texture fabrication in this study, the laser system was operated at a wavelength of 532 nm, a pulse duration of 10 ps, a repetition frequency of 100 kHz, and a focal length of 286 mm. The beam spot diameter was 15 μm, the scanning speed was 100 mm/s, the hatch

spacing was 5 μm, and the number of scan passes was 2. The laser power varied within the range of 0.2–0.5 W depending on the target texture parameters. Prior to coating deposition, the textured surfaces underwent degreasing, rust removal, and polishing treatments. By tuning the average laser power, scan passes, and hatch spacing, textures with the target groove dimensions (depth ~15 μm, width ~120 μm, spacing ~500 μm) were obtained for subsequent coating deposition and testing [11]. The linear, circular, and square textures (Coating-T1, -T2, -T3) were all fabricated with these identical groove dimensions.

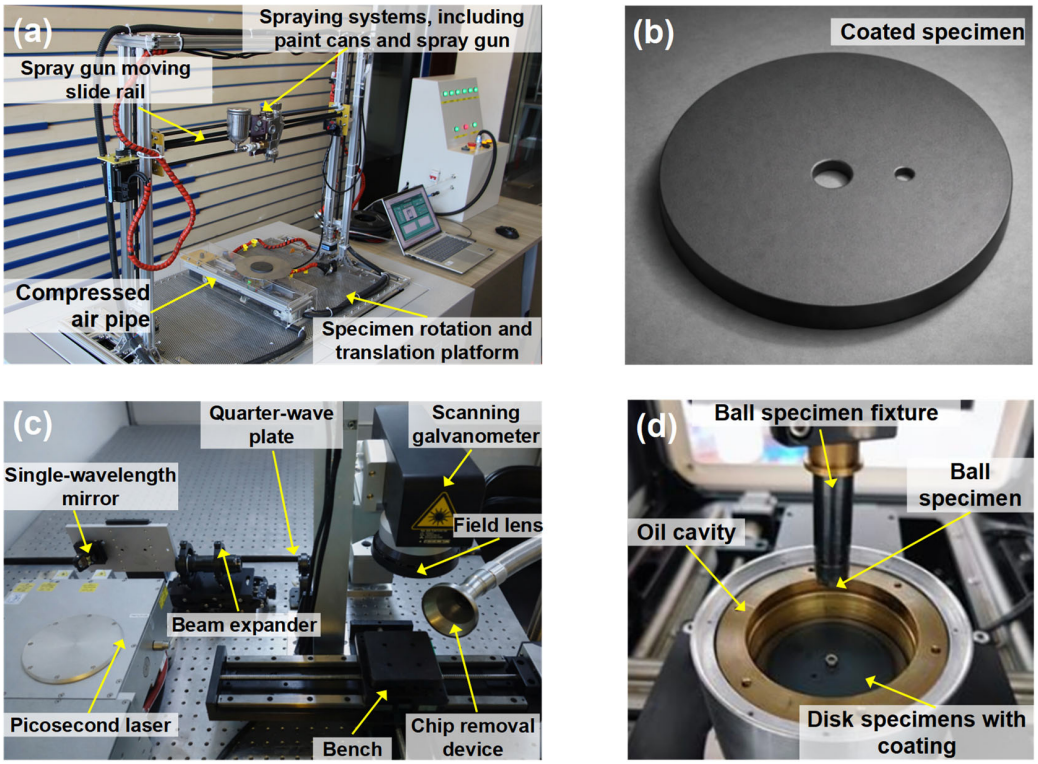


Figure 1. (**a**) Coating spraying equipment. (**b**) Coating physical picture. (**c**) Picosecond laser texturing equipment. (**d**) Ball-on-disk friction and wear test equipment.

The corresponding coatings for these different metal substrate pretreatments are labeled as Coating-P (mechanical polishing), Coating-S (sandblasting process), Coating-T1 (PLST-linear texture), Coating-T2 (PLST-circular texture), and Coating-T3 (PLST-square texture), respectively. As shown in Table 2 and Figure 2, the surface roughness and morphological characteristics after different metal substrate pretreatments are presented. Among them, mechanical polishing was sequentially performed using 800-grit, 1200-grit, and 1500-grit polishing papers on a polishing machine. The sandblasting process employed 120-grit silicon nitride particles, conducted at a distance of 100 mm from the workpiece surface under a pressure of 0.4 MPa.

Table 2. Roughness values of coatings corresponding to different surface pretreatments of metal substrates.

Samples	Coating-P	Coating-S	Coating-T1	Coating-T2	Coating-T3
Ra (μm)	0.156	0.164	0.157	0.148	0.150

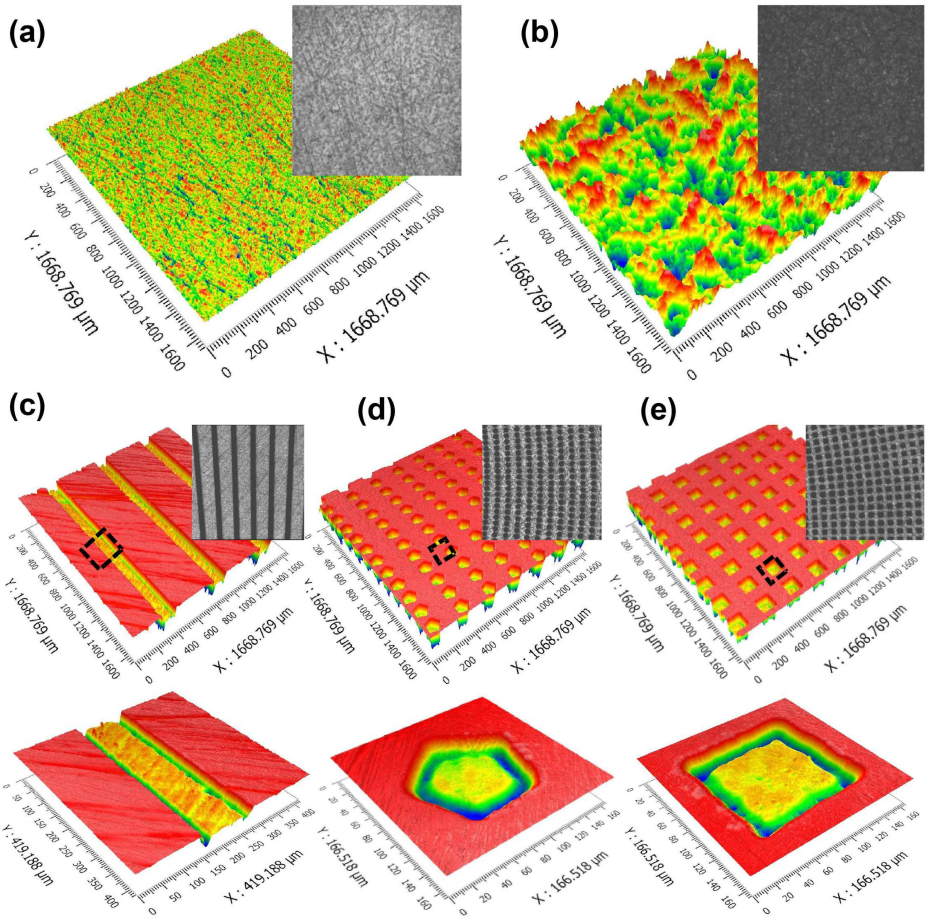


Figure 2. Surface and three-dimensional morphology of (**a**) Coating-P, (**b**) Coating-T1. Laser-textured patterns of (**c**) linear (Coating-T1), (**d**) circular (Coating-T2), and (**e**) square (Coating-T3) textures.

2.2. Tribometry and Wear Track Characterizations

Friction and wear examinations were executed on a ball-on-disk rotating tribometer (Rtec MFT-3000, Rtec Instruments, San Jose, CA, USA), with a relative humidity of 35% ± 5% and an open-air system, as shown in Figure 1d. A bearing steel sphere, 9.6 mm in diameter and 62 ± 2 HRC in hardness, was deployed as the counter-material, boasting a roughness of ~20 nm. The experimental parameters were a temperature of 25 °C, a wear track radius of 10 mm, an applied load of 10 N (corresponding to a maximum Hertzian contact pressure of 1.05 GPa), and a test time of 3600 s. The test rotational speeds were 500, 800, and 1000 rpm.

To examine the resulting wear tracks, a Helios G4 PFIB CXe dual-beam workstation (Thermo Fisher Scientific, Hillsboro, OR, USA) with an integrated EDAX detector (Oxford X-Max 20, Oxford Instruments, Oxford, UK) for energy dispersive X-ray spectroscopy (EDS) was used. Characterization was conducted at a beam current of 1.6 nA and an acceleration voltage of 5 kV. Chemical mapping was performed with 8 cumulative frames.

2.3. Coating Adhesion Tests

To investigate the mechanism by which surface texturing enhances the tribological performance of coatings, this study employed an Rtec SMT-5000 (Rtec Instruments, San Jose, CA, USA) nano-scratch tester to evaluate the coating–substrate bonding strength, which serves as a critical indicator for assessing coating tribological properties and service life. The nano-scratch tests utilized identical substrate materials and coating types as described in Sections 2.1 and 2.2. The scratching experiments were performed in a constant loading-rate mode with linearly increasing normal load, featuring a 5 mm scratch length,

applied load ranging from 0 N to 50 N, and a scratching speed of 0.1 mm/s. A diamond Berkovich indenter (triangular pyramid) with a tip radius of 1 μm was employed for the scratch tests. Post-scratch characterization was conducted using scanning electron microscopy to analyze the microscopic morphology and elemental distribution within the scratched regions. For clarity in the following figures, representative SEM morphologies are shown for a typical segment of the scratch track.

3. Result and Discussion

3.1. Solid Lubricant Coating Characterization

Microstructural and chemical composition analyses were performed on coatings prepared on substrates subjected to three pretreatment methods—mechanical polishing (Coating-P), sandblasting (Coating-S), and picosecond laser texturing (Coating-T1)—as shown in Figure 3. Since the laser-textured patterns were covered by the sprayed coating and therefore do not directly appear in the top-surface SEM morphology, Coating-T1 was selected as the representative sample for detailed surface-phase distribution analysis. Under 100× and 1000× magnification, all coating surfaces exhibited relatively smooth characteristics while retaining regular scratch patterns from post-polishing treatment. Further examination of the morphology and elemental distribution in Figure 3f,g revealed distinct compositional characteristics: Mg, Si, and O elements showed large-area aggregated distribution, while Mo, S, and C elements displayed finer dispersed patterns. This observation indicates that the MSH components in the coating system tend to form aggregated structures within the composite material, whereas MoS_2 and graphite are more dispersed within the matrix.

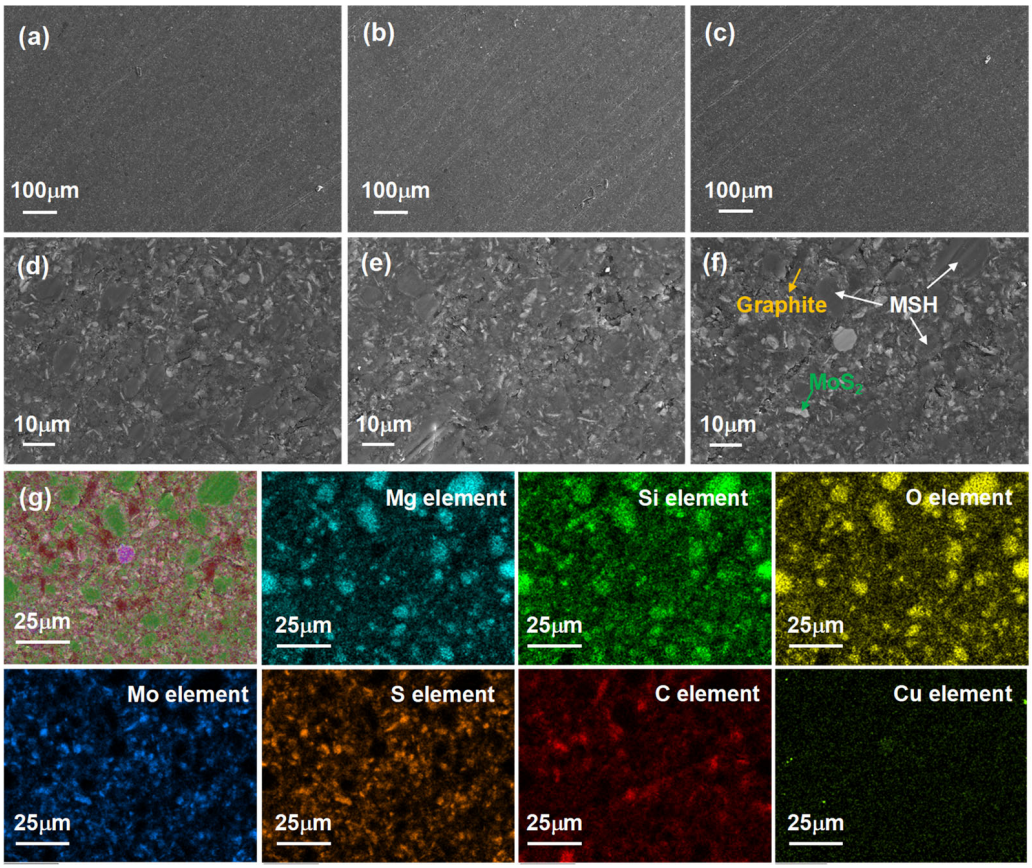


Figure 3. Surface morphologies of (**a**,**d**) Coating-P, (**b**,**e**) Coating-S, and (**c**,**f**) Coating-T1. Panels (**a**–**c**) and (**d**–**f**) correspond to magnifications of 100× and 1000×, respectively. (**g**) Corresponding three-dimensional EDS elemental mapping of Coating-T1 for the region shown in (**f**).

From a laser-processing perspective, PLST defines the interfacial topography before spraying. Cross-sectional observations (Figure 4) confirm that the laser-written groove geometry is preserved at the substrate interface. Therefore, this study focuses on the solid lubricant coating corresponding to linear surface texturing (Coating-T1), with samples prepared using the spraying process described in Section 2.1. Systematic analysis was conducted on the cross-sectional morphology, thickness, and elemental distribution (Figure 4). As shown in Figure 4(a,b1–b8), the textured morphology within the coating matches the white-light 3D topography measurements in Figure 2c: the linear texture features a central depth of approximately 15 μm with a surface width of ~120 μm. Due to picosecond laser ablation characteristics and edge accumulation effects, the depth slightly increases at both edges of the groove, with an adjacent texture spacing of about 500 μm.

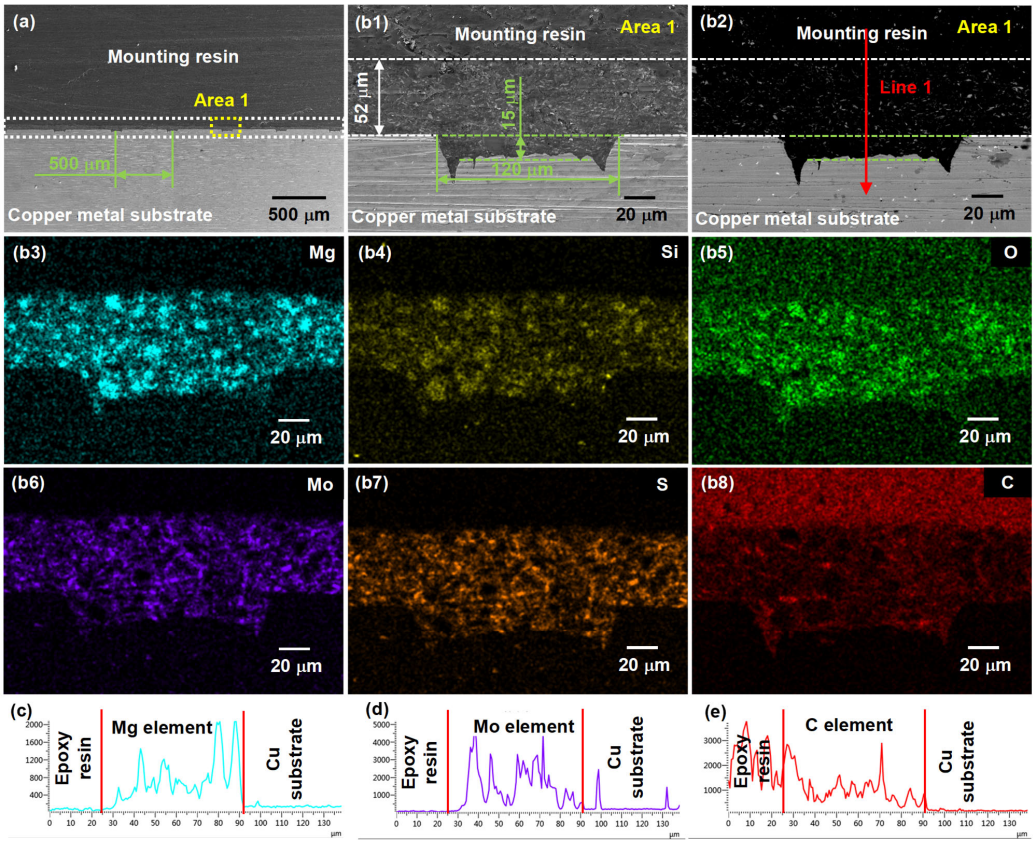


Figure 4. (**a**) and (**b1**) Cross-sectional morphologies of Coating-T1 at 30× and 500× magnification, respectively. (**b2**) Backscattered electron (BSE) image showing atomic number contrast. (**b3**–**b8**) Corresponding EDS elemental maps of the region shown in (**b1**,**b2**). Line-scan analysis along Line 1 in (**b2**) illustrates the through-thickness distribution of (**c**) Mg (indicative of the MSH phase) and (**d**) Mo (indicative of the MoS_2 phase) and (**e**) C (representing graphite phase).

Analysis of elemental mapping (Figure 4(b3–b8)) and elemental distribution curves along the texture depth direction (Figure 4c,d) revealed that characteristic elements of MSH (Mg, Si, O) and Mo/S elements from MoS_2 were distributed throughout both the groove region and the coating matrix, while the carbon signal from graphite remained relatively lower. Notably, consistent with observations in Figure 3g, MSH tended to exist as aggregates within the coating, whereas MoS_2 exhibited a more dispersed distribution pattern. These results confirm the distinct distribution characteristics of different lubricating phases and indicate that the groove regions can serve as phase-rich reservoirs embedded in the coating–substrate interfacial architecture.

3.2. Tribometry and Wear Track Characterization

Under the experimental conditions of 10 N and 800 rpm, Figure 5 systematically compares the tribological performance differences of composite coatings containing the MSH lubricating phase on copper metal substrates subjected to three pretreatment processes: mechanical polishing, sandblasting, and picosecond laser texturing. As shown in the friction coefficient evolution curves in Figure 5a, all three types of coatings exhibit typical "run-in to stable" wear characteristics. The friction coefficient rapidly rises to a peak during the initial stage before gradually decreasing and stabilizing. This phenomenon is attributed to minor wear caused by significant Hertzian contact pressure and shear forces during initial contact. With the continuous release of lubricating phases including graphite, MoS_2, and MSH, the friction coefficient eventually reaches a stable state. Notably, Coating-T1 demonstrates the most excellent friction-reducing performance, with a stable-stage friction coefficient of only 0.038, significantly lower than that of Coating-P (0.048) and Coating-S (0.052).

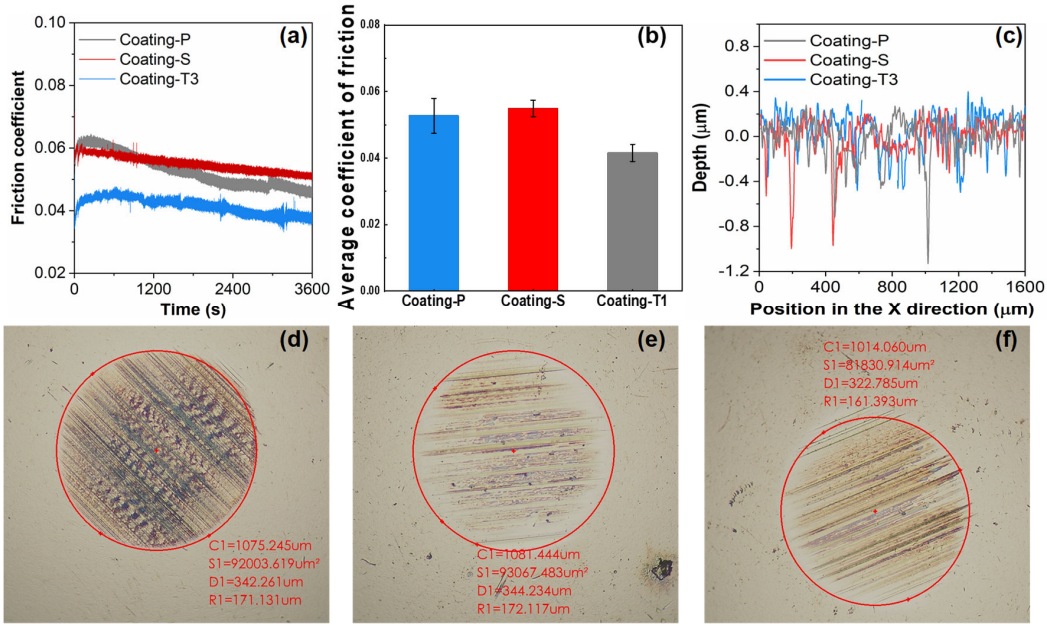


Figure 5. (**a**) The variation in the friction coefficient with the sliding time, (**b**) average friction coefficient obtained on copper metal substrates subjected to three pretreatment processes under the experimental conditions of 10 N and 800 rpm, and (**c**) the cross-sectional depth profile across the wear track for Coating-P, Coating-S, and Coating-T1 obtained at test conditions of 10 N and 800 rpm. The wear scar optical morphologies of the corresponding ball samples: (**d**) Coating-P, (**e**) Coating-S, and (**f**) Coating-T1.

Analysis of the cross-sectional profiles of wear scars in Figure 5c reveals that under the friction conditions of 10 N and 4.8×10^4 revolutions (corresponding to 3600 s at 800 rpm), none of the three coatings show catastrophic material removal. However, the surface morphology of Coating-T1 is the smoothest, with noticeably fewer high-frequency scratch peaks in the wear scar area compared to the other two groups. This result is corroborated by the corresponding ball sample wear scar morphology shown in Figure 5d–f. The wear scar diameter for Coating-T1 (322.8 μm) is approximately 6% smaller than that of Coating-P (342.3 μm) and Coating-S (344.2 μm). This demonstrates that picosecond laser texturing pretreatment can effectively improve the tribological performance of coatings, while the modification effect of conventional mechanical polishing and sandblasting is relatively limited under the same sliding conditions.

Figure 6 displays the morphologies of the three different composite coatings after friction tests at 10 N and 800 rpm. For Coating-P (mechanically polished pretreatment),

the wear was the most severe, with noticeable material spalling observed in the wear scar region (Figure 6a). High-magnification microscopic examination (Figure 6d) further revealed a network of microcracks within the coating. This damage characteristic indicates that the material underwent brittle fracture and local delamination during the friction process. In contrast, Coating-S (sandblasted pretreatment) exhibited significantly reduced wear (Figure 6b), though localized short cracks and material smearing caused by plastic deformation were still observed (Figure 6e). This suggests that while its wear resistance outperformed Coating-P, insufficient coating–substrate bonding strength remained a limiting factor for suppressing microcrack initiation under cyclic shear. Meanwhile, Coating-T1 (picosecond laser-textured pretreatment) demonstrated the best wear resistance (Figure 6c). Its wear scar boundaries were indistinct, with almost no observable spalling on the surface. High-magnification imaging (Figure 6f) confirmed a dense coating structure with no obvious cracks or delamination. These results further validate that picosecond laser texturing pretreatment enhances interfacial bonding and structural integrity of the coating, effectively suppressing crack initiation and propagation during wear.

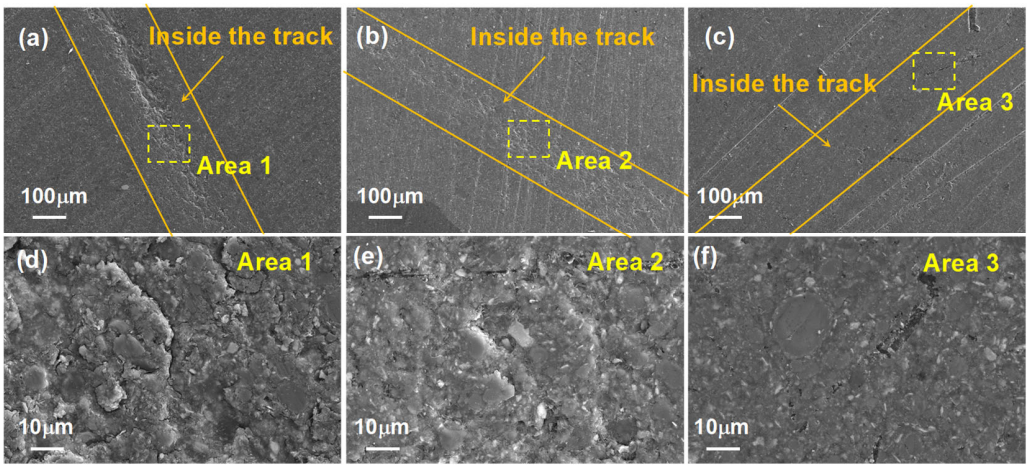


Figure 6. Morphological of the worn surfaces for (**a**,**d**) Coating-P, (**b**,**e**) Coating-S, and (**c**,**f**) Coating-T1 at 100× and 500× magnification.

This study systematically investigates the influence of three micro-texture morphologies (linear, circular, and square) on the tribological performance of coatings, aiming to identify the optimal texture shape. Figure 7a–c present the friction coefficient evolution curves of three textured coatings (Coating-T1/T2/T3) under different rotational speeds of 500, 800, and 1000 rpm. The results demonstrate that, within the tested parameter range, the linear-textured coating consistently exhibits the best tribological performance, maintaining a stable average friction coefficient between 0.045 and 0.053 (Figure 7d), which is significantly lower than those of square- and circular-textured coatings. Notably, when the rotational speed increases to 1000 rpm, the circular-textured (Coating-T2) and square-textured (Coating-T3) coatings show a sharp rise in friction coefficient after 8.6×10^3 and 2.1×10^3 cycles, respectively, indicating coating failure and substrate exposure. In contrast, the linear-textured coating maintains stable frictional performance even under these severe sliding conditions, confirming its superior wear resistance and friction-reducing properties. These findings provide direct experimental evidence for optimizing the surface texture design of coatings and highlight the advantages of linear micro-textures in enhancing durability and tribological efficiency.

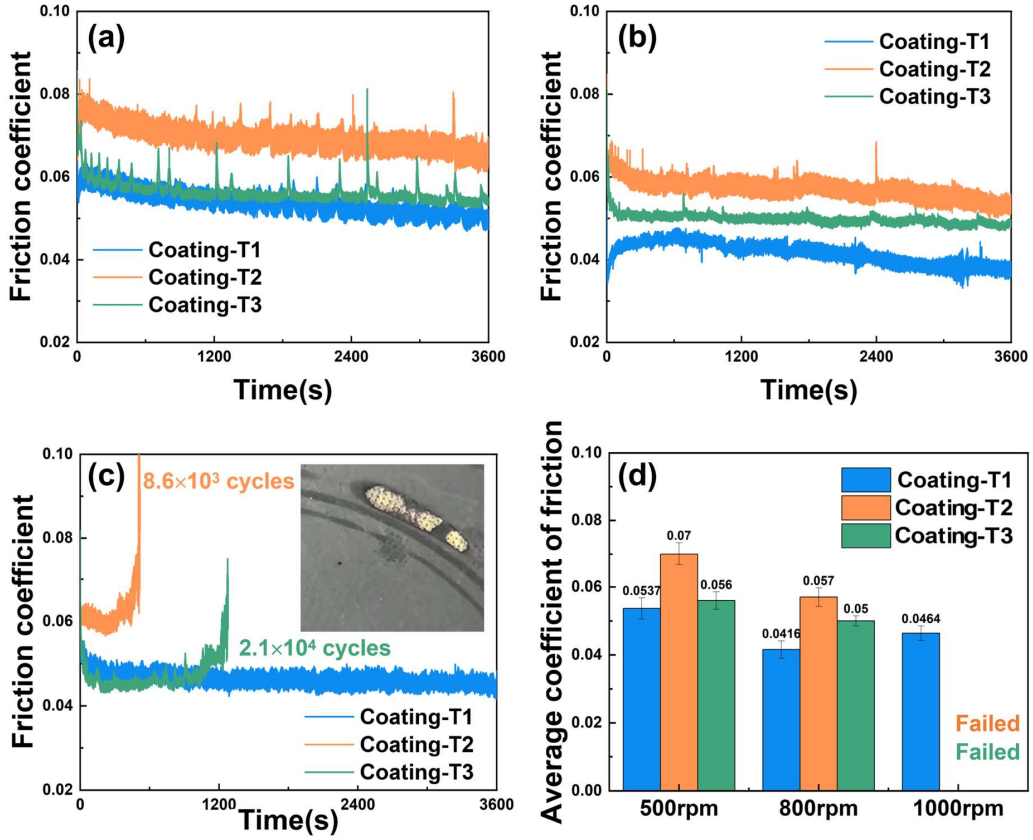


Figure 7. (**a**–**c**) The variation in the friction coefficient with the sliding time for three different coatings at test conditions of 500, 800, and 1000 rpm, respectively. Inset in (**c**) is the photograph of samples showing copper substrate exposure after failure of Coating-T2. (**d**) Average friction coefficient obtained at different rotational speeds.

3.3. Mechanism Analysis

Figure 8a–c respectively present the electron micrographs of the scratches on the surfaces of Coating-P, Coating-S, and Coating-T1, under progressive loading conditions (0–50 N, loading rate 0.1 mm/s). The corresponding evolution curves of the normal force and friction coefficient versus loading time are also shown. A comparison of the three sets of images reveals that as the load increases, the friction coefficients of all three coatings initially rise to a peak of approximately 0.3, followed by fluctuations within a certain range. Notably, Coating-P almost completely delaminates from the copper substrate after the load reaches 7.05 N, and its friction coefficient stabilizes between 0.25 and 0.30, consistent with extensive coating removal and direct copper participation in sliding.

Further analysis of the fluctuation ranges of the friction coefficients for Coating-S and Coating-T1 in the later stages shows that the upper and lower limits of the friction coefficient correspond to exposed copper regions and residual coating regions, respectively. Coating-S exhibits high-frequency fluctuations, consistent with the dense asperities introduced by sandblasting (Figure 2b). Although the arithmetic roughness (Ra) is comparable (Table 2), the peak-to-valley height (Rz/Rt) of the sandblasted surface is much larger (on the order of tens of micrometers), leading to discontinuous lubricant retention and frequent exposure of local copper areas during scratching, its ability to trap and continuously retain lubricating materials (graphite, MoS_2, and MSH) is limited; therefore, the minimum friction coefficient remains between 0.20 and 0.25. In contrast, Coating-T1 does not rely solely on random roughness to capture lubricating phases. Instead, it leverages designed microgrooves (depth ~15 μm, width ~120 μm, spacing ~500 μm; Figures 2d and 4) to provide more effective phase retention and replenishment pathways along the scratch/sliding direction, thereby

reducing the minimum friction coefficient to 0.15–0.22 in the later stage of scratching. Furthermore, based on whether the coating delaminates to expose the copper substrate, the adhesion strengths of Coating-P, Coating-S, and Coating-T1 to the substrate are determined to be 7.05 N, 15.85 N, and 26.05 N, respectively. This result provides a direct explanation for the friction behaviors shown in Figures 5 and 7, indicating that linear texturing significantly enhances the friction-reducing and anti-wear properties of the coating compared with mechanical polishing and sandblasting.

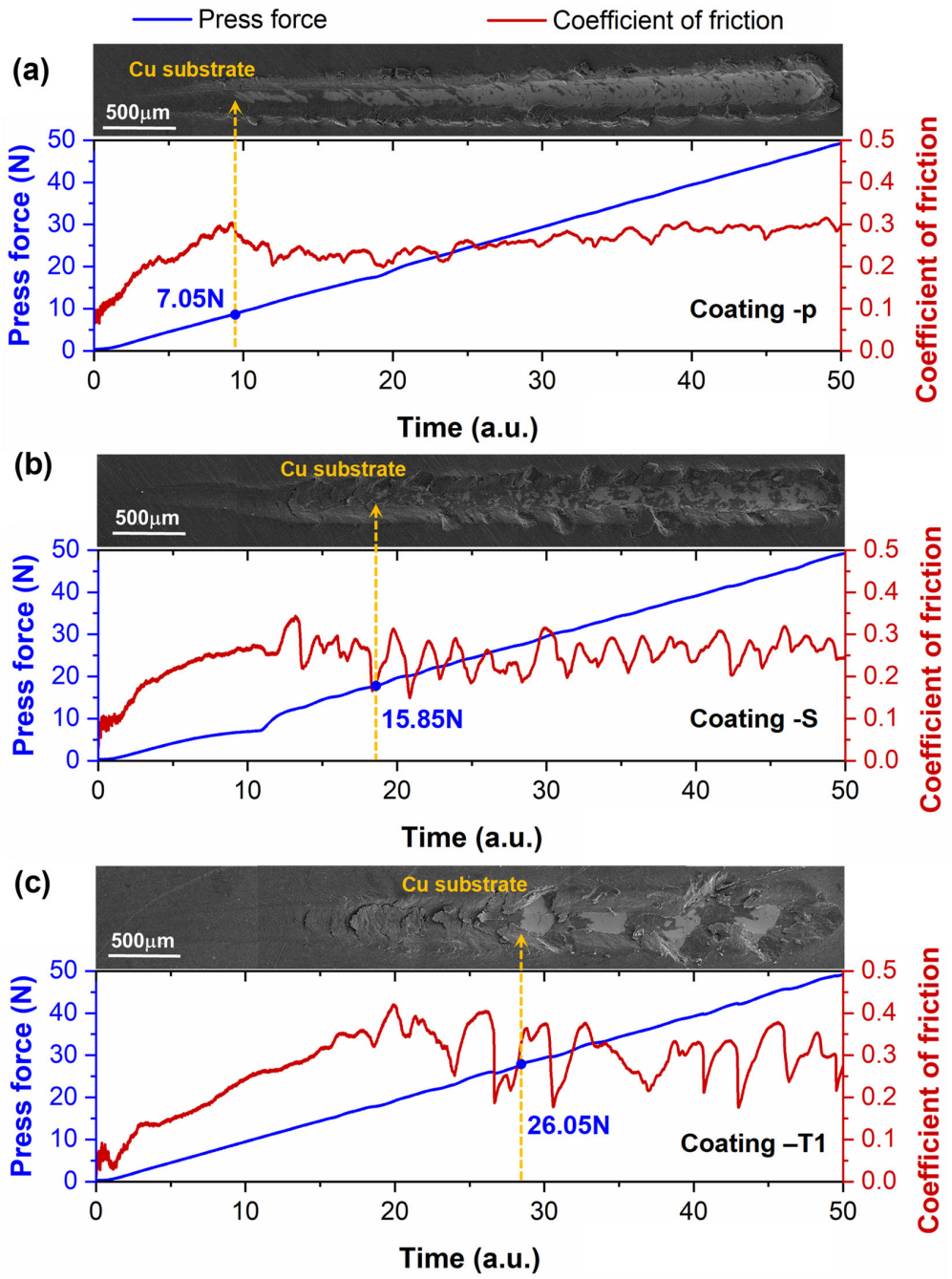


Figure 8. During the scratch testing process, the evolution curves of the normal force and friction coefficient versus scratching time, along with the microscopic morphology of the scratches, are presented. Figures (**a**–**c**) correspond to the scratch results for Coating-P, Coating-S, and Coating-T1, respectively. The critical load for coating–substrate adhesion is determined based on the exposure of the copper substrate, which is marked in the figures.

Figure 9a,b present the electron micrographs of scratches made by a conical indenter on the surfaces of Coating-T2 and Coating-T3 under identical test conditions, along with the corresponding evolution curves of normal force and friction coefficient versus loading time. When the load gradually increases to 21.21 N, the coating corresponding to the circular texture begins to delaminate. Moreover, during subsequent scratching, it fails to achieve the capture and replenishment of lubricating materials, resulting in the friction coefficient consistently remaining above 0.3. As for the square texture, its coating delaminates when the load reaches 23.78 N. Although it exhibits some ability to replenish lubricating materials in subsequent scratching, due to its lower adhesion strength compared to the coating with linear texture, it still demonstrates inferior friction-reducing and anti-wear performance.

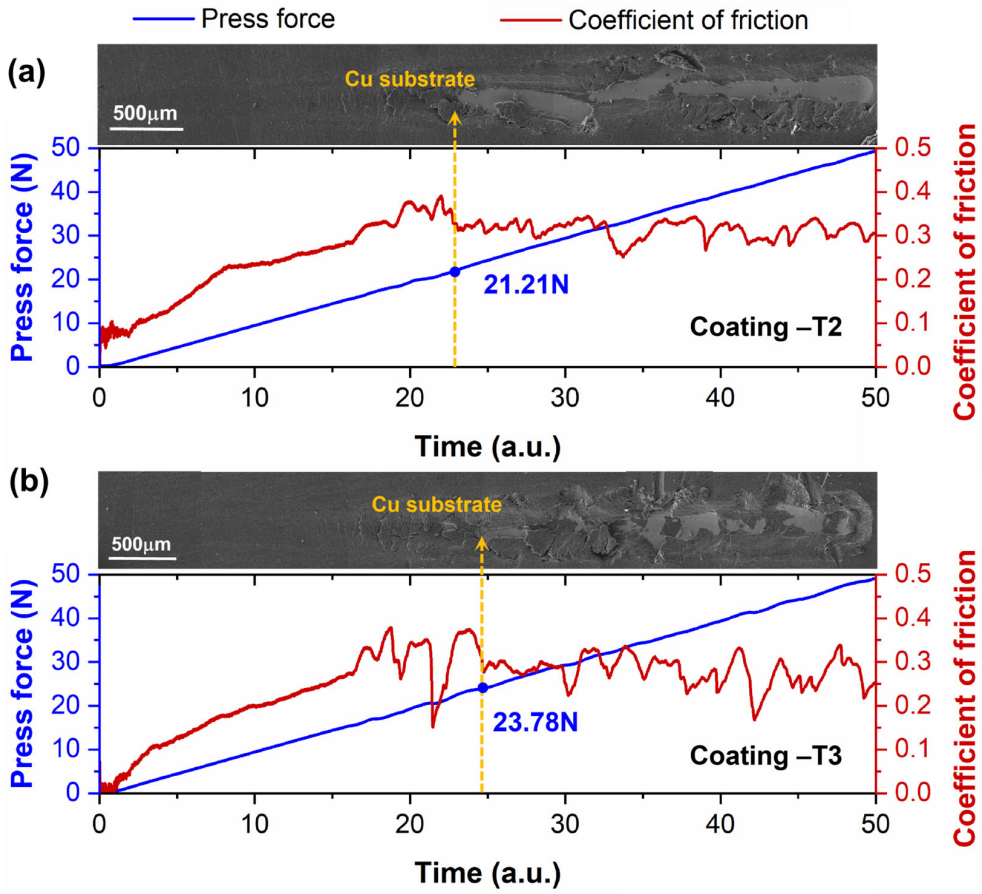


Figure 9. During the scratch testing process, the evolution curves of the normal force and friction coefficient of the conical indenter versus scratching time, along with the microscopic morphology of the scratches for (**a**) Coating-T2 and (**b**) Coating-T3. The critical load for coating–substrate adhesion is determined based on the exposure of the copper substrate, which is marked in the figures.

Figure 10 shows the morphological and elemental distribution analysis performed on Coating-T1 in a region close to substrate exposure after the scratch test. As the loading depth increased, cracks within the coating gradually multiplied, accompanied by the appearance of extrusion wrinkles. These cracks were primarily distributed along both sides of the scratch and extended inward with increasing load. Elemental mapping analysis of Area 1 revealed that, although the coating was severely damaged by the indenter action, elements such as Mg, Si, O, Mo, S, and C were still adhered to the copper substrate surface. This indicates that lubricating phases composed of MSH, MoS_2, and graphite can be retained within the designed surface textures and continuously replenished during sliding/scratching, thereby contributing to friction stabilization and suppression of catastrophic delamination. In combination with the enhanced critical load and the reduced wear

damage morphology, the overall mechanism can be summarized as follows: picosecond laser-induced microgrooves improve (i) mechanical interlocking at the coating–substrate interface and (ii) lubricating phase storage/transport, which together enhance adhesion and tribological durability.

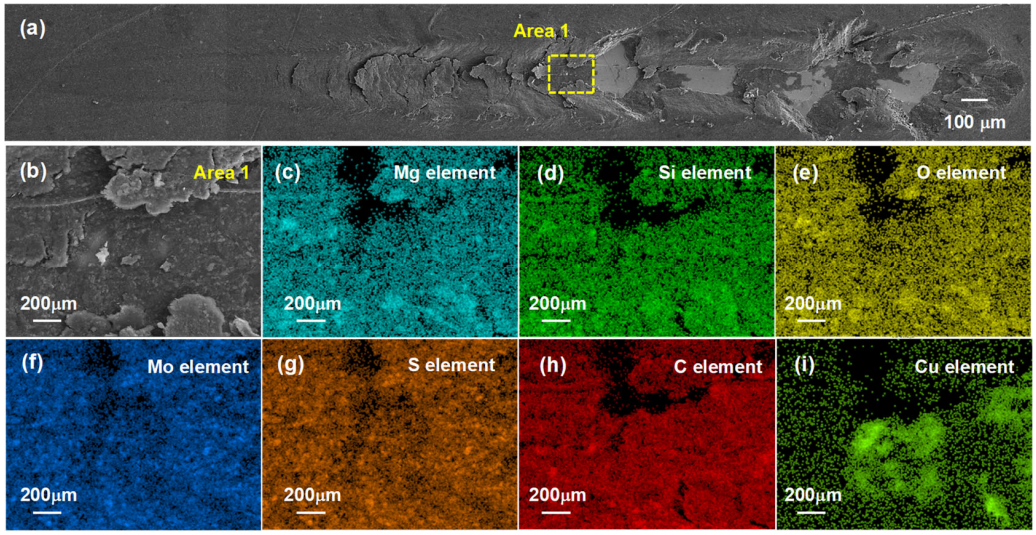


Figure 10. (**a**,**b**) Surface morphologies and (**c**–**i**) corresponding EDS elemental mapping of Coating-T1 after nano-scratch test.

The experimental results above can be rationalized by considering contact mechanics. The nominal Hertzian contact pressure under 10 N is 1.05 GPa (Section 2.2). The presence of microgrooves modifies this stress distribution: stress concentration at groove edges enhances mechanical interlocking, while the reduced real contact area lowers effective friction. As illustrated in the lower-right inset of Figure 11, under load the counter-surface undergoes local elastic deformation, pressing coating material into the microgrooves to form mechanical anchors. Cyclic sliding also pumps solid lubricants from the grooves to the interface.

Based on this contact-mechanical understanding, the PLST-fabricated linear microgrooves act as a parameter-controlled interfacial architecture that (i) provides mechanical interlocking, retarding crack initiation and delamination, and (ii) serves as phase-rich reservoirs, continuously supplying lubricants to the sliding contact. During running-in, stored lubricants are gradually released, facilitating a stable transfer film and stabilizing friction. Under kerosene-contaminated conditions, the grooves also promote lubricant entrainment and mitigate starvation. Overall, the synergy of interfacial strengthening and lubricant retention accounts for the lower friction and enhanced adhesion of Coating-T1.

Building on these kerosene-contaminated results, it is instructive to consider how the proposed mechanisms might behave under other lubrication regimes. Under fully dry sliding, the absence of fluid-assisted transport could reduce lubricant replenishment from the groove reservoirs, potentially shortening wear life. In oil-lubricated environments, the microgrooves may additionally promote hydrodynamic effects, though compatibility with solid lubricants would need further study. The present findings are limited to the tested conditions (load, speed, counter-material, and kerosene contamination); broader applicability remains to be verified.

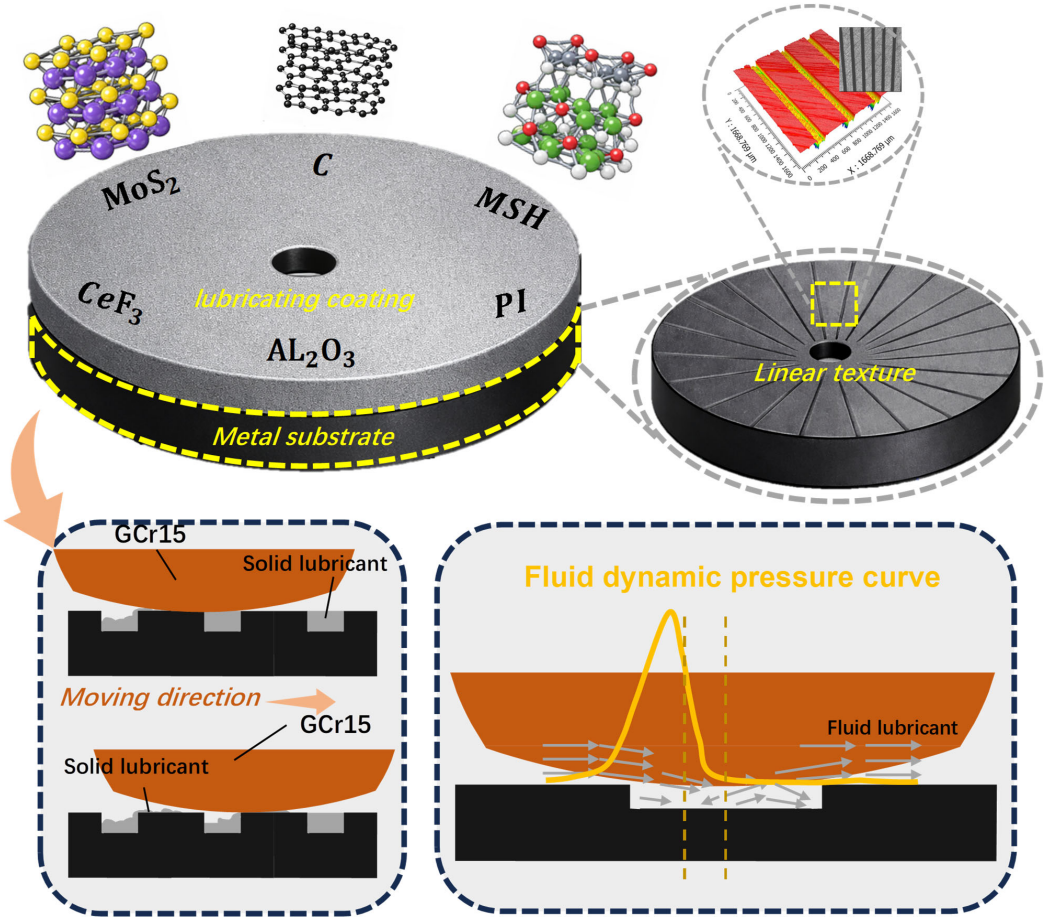


Figure 11. Schematic illustration of the friction-reduction and adhesion-enhancement mechanisms enabled by linear laser microgrooves in Coating-T1.

4. Conclusions

In conclusion, this paper focuses on an MSH-containing solid lubricant coating prepared on copper substrates and investigates the effects of substrate texturing pretreatment (via picosecond laser) on the friction coefficient, wear behavior, and coating–substrate adhesion. Ball-on-disk tests in a kerosene-contaminated environment show that texturing pretreatment significantly reduces the steady-state friction coefficient and improves wear resistance compared to traditional mechanical polishing and sandblasting. Nano-scratch tests further demonstrate a marked increase in the critical load for coating failure, indicating enhanced interfacial adhesion. This improvement is primarily attributed to (i) mechanical interlocking facilitated by the designed microgrooves and (ii) storage and sustained release/replenishment of lubricating phases. Furthermore, the study reveals that the texture shape has a significant impact on tribological performance: linear microgrooves provide the most stable friction and the highest adhesion among the three investigated geometries (linear, circular, and square). These findings support the use of textured substrate pretreatment as an effective strategy for improving the reliability of solid lubricant coatings under severe sliding conditions, and they offer guidance for texture-shape optimization. From a tribological optimization perspective, the results highlight that well-designed interfacial micro-textures (fabricated via maskless and controllable picosecond laser processing with limited thermal influence) are crucial for governing coating adhesion and tribological stability.

Author Contributions: B.G. conceived and designed the study. Q.C. participated in the conceptualization of the research. B.G., H.Y., Z.W., X.W., P.B. and Z.T. were responsible for the methodology. B.G. performed the software analysis. B.W. conducted the data curation. B.G. and H.Y. wrote the original draft. H.Y. and R.L. revised and edited the manuscript. Q.C. acquired the funding. Meanwhile, B.G. performed the experiments and simulations. B.W. analyzed the data. B.G. and H.Y. contributed equally and share first authorship. All authors have read and agreed to the published version of the manuscript.

Funding: This research used resources of the Talent Fund of Beijing Jiaotong University (Contract No. M23XKRC00020), the National Natural Science Foundation of China (Grant No. 52005284), the Financial Program of BJAST (Contract No. 24CB011-01), the Tribology Science Fund of State Key Laboratory of Tribology (Grant No. SKLTKF21A02), the Research Institute of Petroleum Processing, Sinopec (Contract No. 3360000-22-ZC0699-0079), and National Key Research and Development Program of China (Contract No. 2022YFB3402904).

Data Availability Statement: All data presented in this study were obtained from original experiments.

Conflicts of Interest: Author Zhenyu Tian was employed by Shandong Metallurgical Machinery Factory Co., Ltd. The remaining authors declare that the research was conducted in the absence of any commercial or financial relationships that could be construed as a potential conflict of interest.

Nomenclature

PLST	Picosecond laser surface texturing
MSH	Magnesium silicate hydroxide
PI	Polyimide
DMF	Dimethylformamide
ps/fs	Picosecond/femtosecond
Coating-P	Coating on mechanically polished copper substrate
Coating-S	Coating on sandblasted copper substrate
Coating-T1	Coating on linear-textured copper substrate
Coating-T2	Coating on circular-textured copper substrate
Coating-T3	Coating on square-textured copper substrate
HRC	Rockwell hardness C scale
Lc	Critical load for coating delamination

References

1. Liu, J.L.; Wang, Y.S.; Yu, C.B. Few-layer MoS_2 modified epoxy/MoS_2-graphite coating: Robust solid lubrication enabling sustained tribological performance during oil lubrication failure. *Surf. Interfaces* **2025**, *72*, 12. [CrossRef]
2. Colas, G.; Saulot, A.; Philippon, D.; Berthier, Y.; Léonard, D. Tribochemical Competition within a MoS_2/Ti Dry Lubricated Macroscale Contact in Ultrahigh Vacuum: A Time-of-Flight Secondary Ion Mass Spectrometry Investigation. *ACS Appl. Mater. Interfaces* **2018**, *10*, 20106–20119. [CrossRef] [PubMed]
3. Wang, J.F.; Xue, W.H.; Gao, S.Y.; Li, S.; Duan, D.L. Effect of groove surface texture on the fretting wear of Ti-6Al-4V alloy. *Wear* **2021**, *486*, 11. [CrossRef]
4. Xu, J.; Dai, J.; Ren, F.Z.; Wang, Y.F.; Wang, P.; Xu, S.S.; Wu, S.; Lin, J.; Yang, Y.; Guo, D.; et al. Ultrahigh radiation resistance of nanocrystalline diamond films for solid lubrication in harsh radiative environments. *Carbon* **2021**, *182*, 525–536. [CrossRef]
5. Kumar, R.; Hussainova, I.; Rahmani, R.; Antonov, M. Solid Lubrication at High-Temperatures—A Review. *Materials* **2022**, *15*, 27.
6. Feng, X.; Wang, R.; Wei, G.; Zheng, Y.; Hu, H.; Yang, L.; Zhang, K.; Zhou, H. Effect of a micro-textured surface with deposited MoS_2-Ti film on long-term wear performance in vacuum. *Surf. Coat. Technol.* **2022**, *445*, 128722.
7. Singh, R.A.; Yoon, E.S. Biomimetics in tribology—Recent developments. *J. Korean Phys. Soc.* **2008**, *52*, 656–668. [CrossRef]
8. Liu, D.R.; Zhang, Q.; Qin, Z.B.; Luo, Q.; Wu, Z.; Liu, L. Tribological performance of surfaces enhanced by texturing and nitrogen implantation. *Appl. Surf. Sci.* **2016**, *363*, 161–167. [CrossRef]
9. Zhang, D.Y.; Gao, F.; Wei, X.; Liu, G.L.; Hua, M.; Li, P.Y. Fabrication of textured composite surface and its tribological properties under starved lubrication and dry sliding conditions. *Surf. Coat. Technol.* **2018**, *350*, 313–322.
10. Almonti, D.; Baiocco, G.; Menna, E.; Rubino, G. Enhanced wear resistance in Nickel-graphene-PTFE composite coatings: Fabrication and characterisation. *Surf. Eng.* **2025**, *41*, 383–392. [CrossRef]

11. Lin, G.P.; Yu, G.Y.; Cai, Z.B.; Gu, L.; Dong, Z.; Zhang, P.; Wang, Q.W.; Wang, J.; Yan, X.C.; Lu, B.W. Effect of process parameters on the dimension and morphology of laser cladded WC-Ni composite coatings prepared by picosecond laser surface texturing. *Opt. Laser Technol.* **2026**, *198*, 114874. [CrossRef]
12. Huang, Q.P.; Shi, X.L.; Xue, Y.W.; Zhang, K.P.; Wu, C.H. Recent progress on surface texturing and solid lubricants in tribology: Designs, properties, and mechanisms. *Mater. Today Commun.* **2023**, *35*, 30. [CrossRef]
13. Kim, S.H.; Jeong, S.H.; Kim, T.H.; Choi, J.H.; Cho, S.H.; Kim, B.S.; Lee, S.W. Effects of solid lubricant and laser surface texturing on tribological behaviors of atmospheric plasma sprayed Al_2O_3-ZrO_2 composite coatings. *Ceram. Int.* **2017**, *43*, 9200–9206. [CrossRef]
14. Ahmadzadeh, H.; Isfahani, T.; Kharazi, A.Z. Modified Mechanical Coating Technique for the Preparation of Nanohydroxyapatite Coated Ti-6Al-4V Dental Implants. *Prot. Met. Phys. Chem. Surf.* **2020**, *56*, 766–771. [CrossRef]
15. Huang, Y.; Liu, T.X.; Liu, J.Y.; Li, J. Study on synergistic friction between surface micro-texture and hot-pressing filling coal-to-oil soot solid lubricant. *Surf. Coat. Technol.* **2024**, *489*, 12. [CrossRef]
16. Ma, Y.J.; Chen, L.; Ye, Y.P.; Wan, H.Q.; Zhou, H.D.; Chen, J.M. Preparation and tribological behaviors of a novel organic-inorganic hybrid resin bonded solid lubricating coating cured by ultraviolet radiation. *Prog. Org. Coat.* **2019**, *127*, 348–358. [CrossRef]
17. Li, B.W.; Xu, Z.T.; Duan, G.H.; Yang, X.; Liu, B.; Shao, Y.L.; Liu, M.; Liu, R. The Fluidized Bed-Chemical Vapor Deposition Coating Technology of Micro-Nano Particles: Status and Prospective. *Coatings* **2025**, *15*, 27. [CrossRef]
18. Xian, G.; Xiong, J.; Fan, H.; Guo, Z.; Xian, L.; Sun, L.; Zhao, H. Effect of substrate pretreatments on the structure and properties of AlTiN coatings deposited on TiCN-based cermets. *Thin Solid Film.* **2023**, *770*, 139733. [CrossRef]
19. Zhang, X.H.; Rong, W.T.; Wen, D.D.; Jiang, J.; Shi, Z.Y.; He, T.Z.; Zhou, Z.Y.; Ibrahim, A.M.M. Synergistic improvement of grinding performance in form grinding of titanium alloys using laser combinatorial surface texturing. *Opt. Laser Technol.* **2025**, *189*, 113057. [CrossRef]
20. Bartkowiak, T.; Brown, C.A. A Characterization of Process-Surface Texture Interactions in Micro-Electrical Discharge Machining Using Multiscale Curvature Tensor Analysis. *J. Manuf. Sci. Eng-Trans.* **2018**, *140*, 7. [CrossRef]
21. Shen, Y.; Ye, B.; Yu, B.H.; Liu, Z.X.; Huang, R.X.; Xu, J.J. Enhancement of heavy-duty friction and wear characteristics of cast-iron surface by electrolytic micro-textures filled with MoS_2. *Surf. Coat. Technol.* **2021**, *408*, 11. [CrossRef]
22. Shen, Y.; Lv, Y.T.; Li, B.; Huang, R.X.; Yu, B.H.; Wang, W.W.; Li, C.; Xu, J. Reciprocating electrolyte jet with prefabricated-mask machining micro dimple arrays on cast iron cylinder liner. *J. Mater. Process. Technol.* **2019**, *266*, 329–338. [CrossRef]
23. Etsion, I.; Kligerman, Y.; Halperin, G. Analytical and experimental investigation of laser-textured mechanical seal faces. *Tribol. Trans.* **1999**, *42*, 511–516. [CrossRef]
24. Arenas, M.A.; Ahuir-Torres, J.I.; García, I.; Carvajal, H.; de Damborenea, J. Tribological behaviour of laser textured Ti6Al4V alloy coated with MoS_2 and graphene. *Tribol. Int.* **2018**, *128*, 240–247. [CrossRef]
25. Zhai, Z.Y.; Qu, Y.J.; Zhang, H.M.; Wang, B.; Zhang, Y.C.; Cui, Y.H. Fabrication of microtexture by pulse laser to improve the bonding strength of coating. *Optik* **2022**, *265*, 12. [CrossRef]
26. MacLucas, T.; Grützmacher, P.; Husseini, S.; Leonhard-Trautmann, P.; Suarez, S.; Gachot, C.; Mücklich, F. Combining Carbon Nanoparticle Coatings and Laser Surface Texturing for Enhanced Lubricity Under High Loads. *Tribol. Lett.* **2024**, *72*, 38. [CrossRef]
27. Ilemona, O.S.; Iabbaden, D.; Ganster, P.; Itina, T.E. Reactive atomistic insights into oxidation dynamics and wettability of ultrafast laser-treated titanium surfaces. *Surf. Interfaces* **2025**, *68*, 106537.
28. Ariza, R.; Alvarez-Alegria, M.; Costas, G.; Tribaldo, L.; Gonzalez-Elipe, A.R.; Siegel, J.; Solis, J. Multiscale ultrafast laser texturing of marble for reduced surface wetting. *Appl. Surf. Sci.* **2022**, *577*, 151850. [CrossRef]
29. Shi, Z.; Duan, X.F.; Chen, Z.H.; Liu, B.; Fu, H.; Ji, J.H.; Zhang, Y.H. Precision fabrication of micro-textures array for surface functionalization using picosecond pulse laser. *Opt. Laser Technol.* **2024**, *177*, 111200. [CrossRef]
30. Wu, S.Y.; Wang, Y.H.; Jiang, X.D.; Hu, S.; Yao, C.Z.; Dong, B.; Ma, C.; Lu, L.H.; Chen, J.X. Bioinspired femtosecond laser surface texturing for enhancing tribological properties of Ti6Al4V titanium alloy. *Tribol. Int.* **2026**, *213*, 110987.
31. Souza, F.C.R.; Rossi, W.d.; Silva, L.d.; Paula, F.A.; Machado, S.R. Production and characterization of texture in PCD cutting tools with femtosecond laser: Analysis of texture quality and surface integrity in the turning of AA2011-T4 aluminum. *Tribol. Int.* **2025**, *212*, 110977. [CrossRef]
32. Yu, C.; Li, M.H.; Mu, R.X.; Chen, Z.H.; Cao, X.W.; Li, M.T.; Wang, Y.H.; Li, A.W. Synergistic femtosecond laser direct writing-electrochemical micromachining for ultra-smooth micro-texturing on metallic surfaces. *Opt. Commun.* **2025**, *590*, 132094. [CrossRef]
33. Khan, M.A.; Halil, A.M.; Abidin, M.S.Z.; Hassan, M.H.; Rahman, A.A.A. Influence of laser surface texturing on adhesive bonding: A comprehensive review on surface morphology and strength enhancement. *Opt. Laser Technol.* **2025**, *191*, 113339. [CrossRef]
34. Shi, C.; Chang, Q.; Wang, W.; Liu, M.; Li, Z.; Yan, Q. The effect of spray drying parameters on drying of magnesium silicate hydroxide microspheres. *Powder Technol.* **2024**, *442*, 119882. [CrossRef]

35. Yan, Q.Q.; Chang, Q.Y.; Shi, C.X. Morphology-dependent tribological performance of magnesium silicate hydroxide nanostructures as lubricant additives: A comparative study of plate-like and tubular variants. *Surf. Interfaces* **2025**, *73*, 107496. [CrossRef]
36. Bechikh, A.; Kliniakova, O.; Maalej, Y.; Tawfiq, I.; Nasri, R. Sandblasting parameter variation effect on galvanized steel surface chemical composition, roughness and free energy. *Int. J. Adhes. Adhes.* **2020**, *102*, 102653. [CrossRef]

Disclaimer/Publisher's Note: The statements, opinions and data contained in all publications are solely those of the individual author(s) and contributor(s) and not of MDPI and/or the editor(s). MDPI and/or the editor(s) disclaim responsibility for any injury to people or property resulting from any ideas, methods, instructions or products referred to in the content.